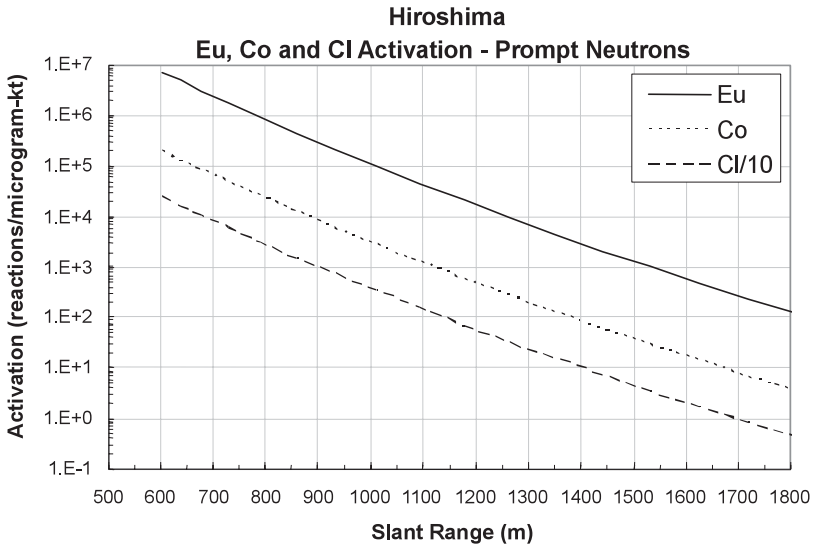

Figure 11. *Activation of Eu, Co and Cl by prompt neutrons vs. slant range (Hiroshima bomb).*

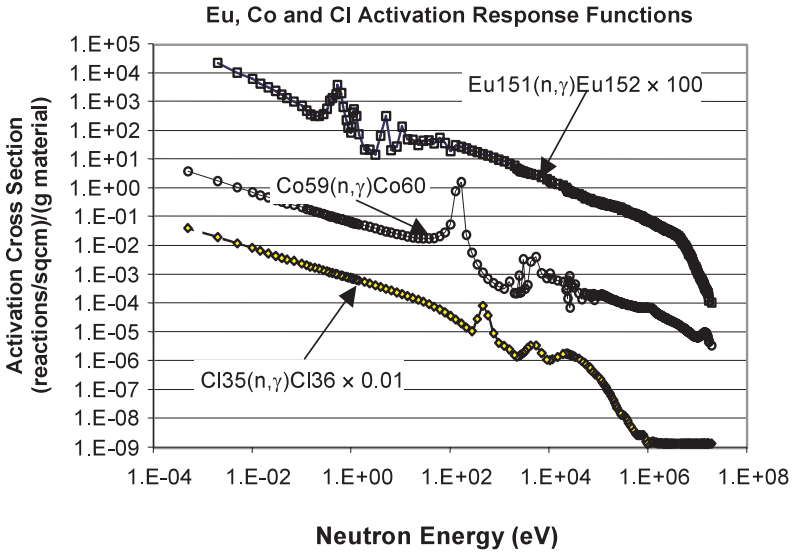

Figure 12. *Eu, Co and Cl activation response functions vs. neutron energy [response functions are given in (reactions/cm^2)/(gram material-kt)].*

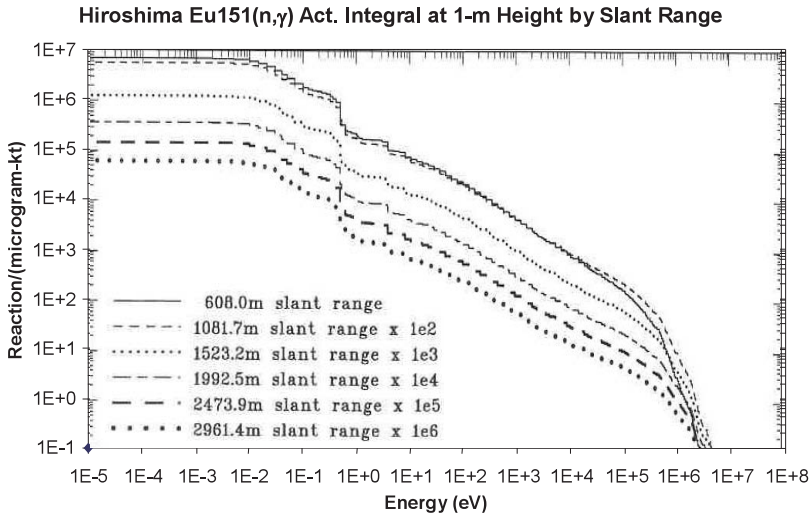

Figure 13. *Energy integrated $^{151}Eu(n,\gamma)^{152}Eu$ activation at 1 m above the ground as a function of neutron energy and slant range (Hiroshima bomb).*

Results of Discrete Ordinates Calculations - Nagasaki Weapon

The prompt radiation discrete ordinates calculations for the Nagasaki bomb were performed for a 503-m HOB. Contours of constant fluence are shown in Figure 14. The fluences are plotted as a function of ground range and altitude above the ground plane and are normalized to a weapon yield of 1 kt. The neutron fluence as well as the primary and secondary gamma-ray fluences are smoothly varying with distance and altitude and, as in the case of the Hiroshima profiles, are all free of ray effects. The prompt neutron, secondary gamma-ray and prompt gamma-ray fluence distributions calculated as a function of energy and slant range at 1 m above the ground, exhibit similar overall behavior as the curves shown in Figures 6 through 8 for the Hiroshima weapon. The neutron and gamma-ray spectra approach equilibrium as the distance from the hypocenter increases.

Figure 15 shows the number of (n,γ) reactions per microgram of ^{59}Co, ^{35}Cl and ^{151}Eu at 1 m above the ground as a function of slant range. These data are normalized to a weapon yield of 1 kt. These data were obtained by folding the neutron fluence with the ^{59}Co-, ^{35}Cl- and ^{151}Eu-(n,γ) response functions shown in Figure 12. The curves exhibit a different exponential decay with slant range. At short slant ranges the curves decrease more rapidly with distance than at Hiroshima. Beyond about 800 m slant range, the prompt reactions decrease less rapidly.

As in the case for the Hiroshima event, the activation of ^{59}Co, ^{35}Cl and ^{151}Eu at Nagasaki is due chiefly to epithermal and thermal neutron capture reactions. This is shown in Figure 16 where the energy integrated $^{151}Eu(n,\gamma)^{152}Eu$ activation at 1 m above the ground is plotted as a function of neutron energy. Ninety percent of the activation of ^{151}Eu is due to reactions of neutrons with energies below about 0.1 eV. The jump in the activation at about 0.5 eV is due to the resonance peak in the response function for ^{151}Eu shown in Figure 12.

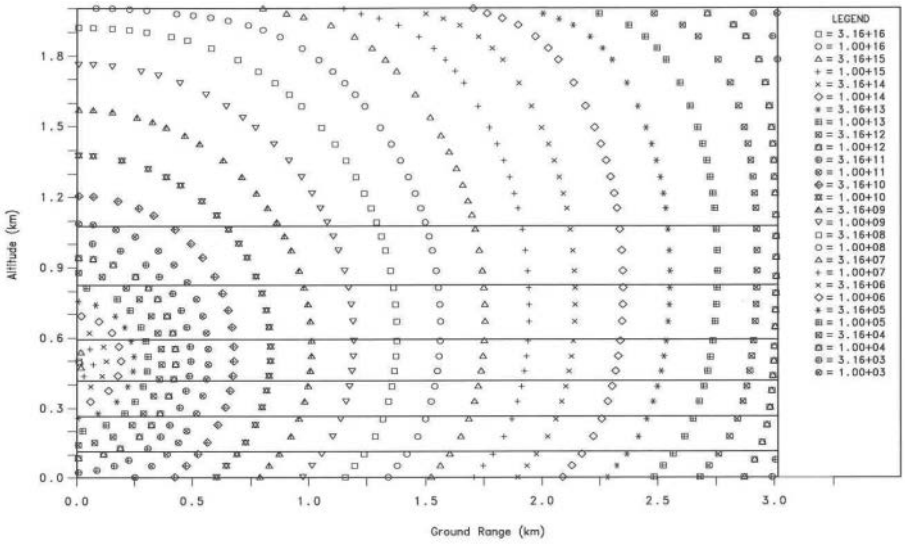

Figure 14. *Contours of constant prompt neutron fluence (Nagasaki bomb).*

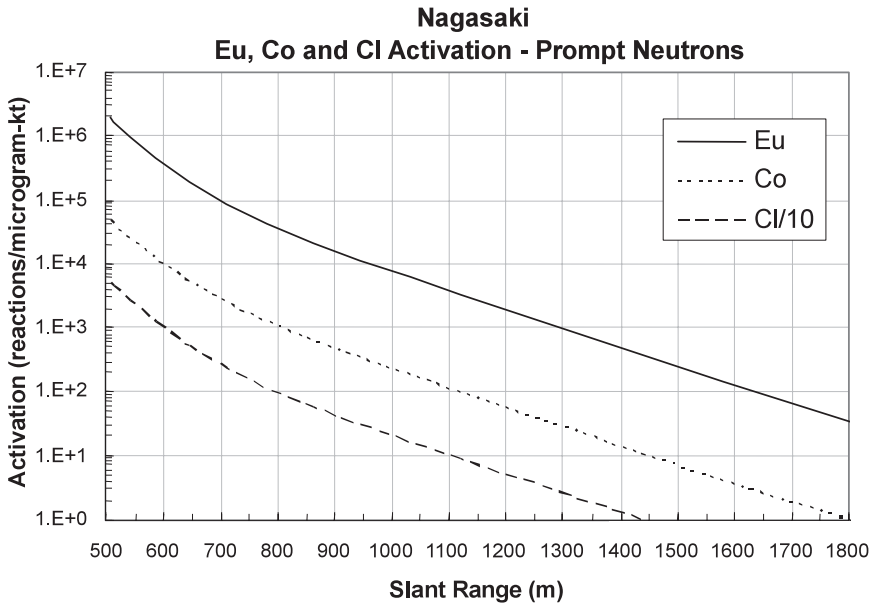

Figure 15. *Activation of Eu, Co and Cl by prompt neutrons vs. slant range (Nagasaki bomb).*

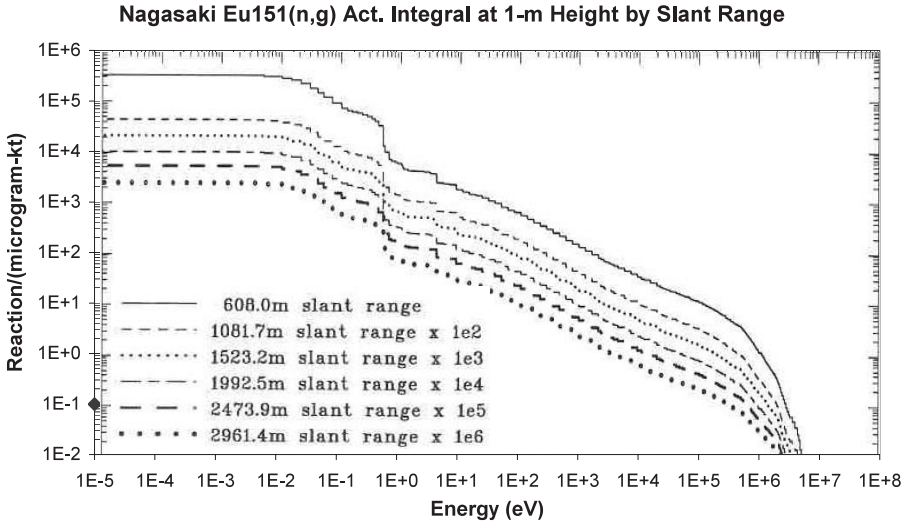

Figure 16. *Energy integrated $^{151}Eu(n,\gamma)^{152}Eu$ activation at 1 m above the ground as a function of neutron energy and slant range (Nagasaki bomb).*

Results of Discrete Ordinates Calculations - Comparisons of Fluence and Activation Data

Figures 17 through 22 compare the Hiroshima and Nagasaki prompt neutron, prompt gamma-ray and secondary gamma-ray fluence per unit lethargy vs. energy at 1 m above the ground. The spectra are compared in the figures at slant ranges of 608 and 1,082 m from the epicenter. The Nagasaki spectra have been scaled to compare the curves in terms of the same number of neutrons to show the differences in the data with slant range.

The Nagasaki spectra were scaled using the following procedure. The total number of particles in each spectrum, Φ_T, was obtained by integrating each spectrum over energy. The Nagasaki spectra were then normalized to the Hiroshima spectra using the relation:

$$\Phi_{Scaled}(E, \text{Nagasaki}) = \Phi(E, \text{Nagasaki}) \times [\Phi_T(\text{Hiroshima})/\Phi_T(\text{Nagasaki})] ,$$

where Φ(E, Nagasaki) is the Nagasaki fluence per unit energy. Normalizing the spectra in this manner allows the spectra to be compared in terms of the same number of particles to show similarities and differences in the spectra as a function of energy.

The Nagasaki neutron spectrum at 608 m slant range in Figure 17 shows a greater number of neutrons at energies greater than 10^6 eV and fewer neutrons in the energy range between $10^{-1}$and 10^5 eV than in the Hiroshima spectrum. As the slant range increases (Figure 18), the spectra have for the most part the same shape at energies up to 10^6 eV and the differences between the spectra at higher energies become smaller. But over the range of these calculations the spectra approach, but never acquire the same shape at high neutron energies. The spectra below 10^5 eV are all very similar in shape and scaled magnitude at all slant ranges and are dominated by the epithermal and thermal neutrons produced in the air and ground.

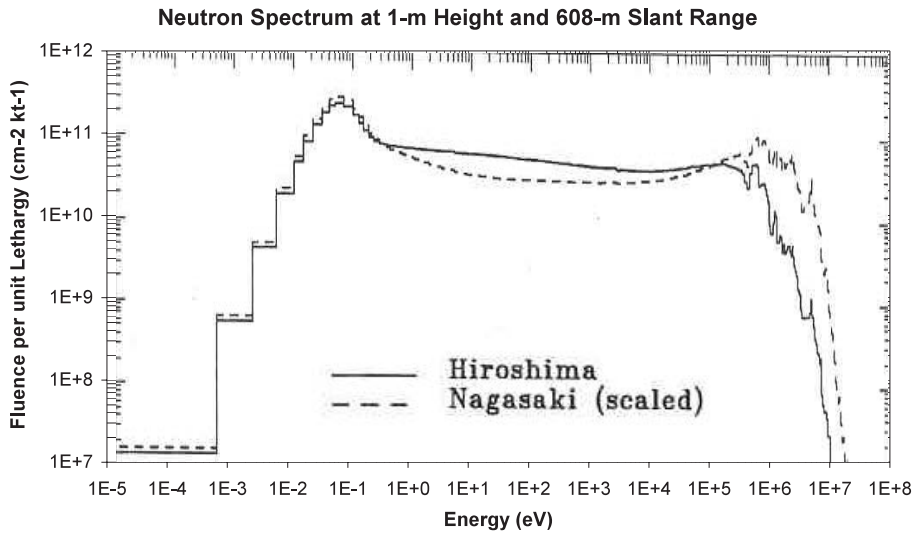

Figure 17. *Comparison of Hiroshima and Nagasaki neutron fluence per unit lethargy vs. neutron energy at a slant range of 608 m.*

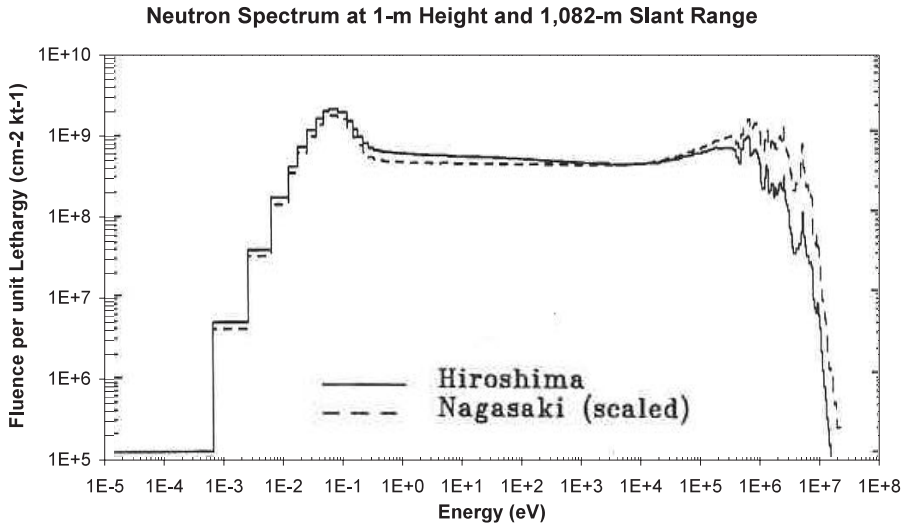

Figure 18. *Comparison of Hiroshima and Nagasaki neutron fluence per unit lethargy vs. neutron energy at a slant range of 1,082 m.*

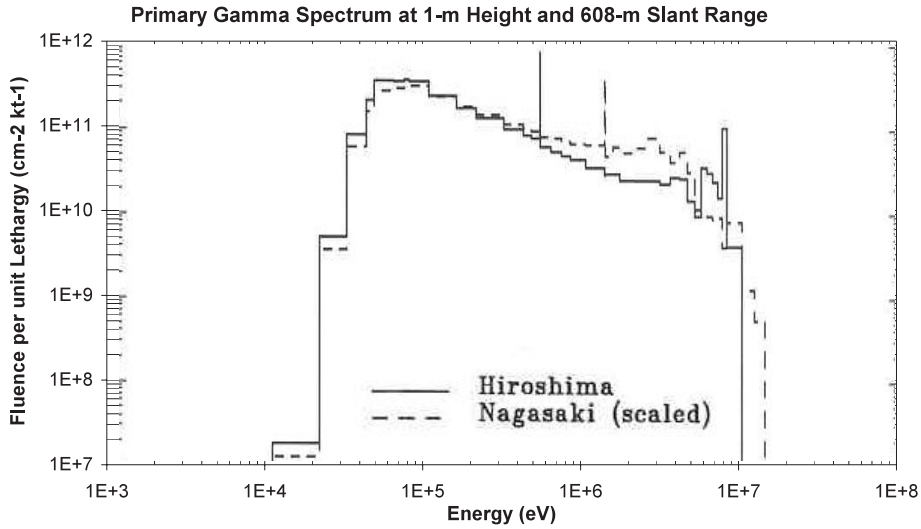

Figure 19. *Comparison of Hiroshima and Nagasaki prompt gamma-ray fluence per unit lethargy vs. neutron energy at a slant range of 608 m.*

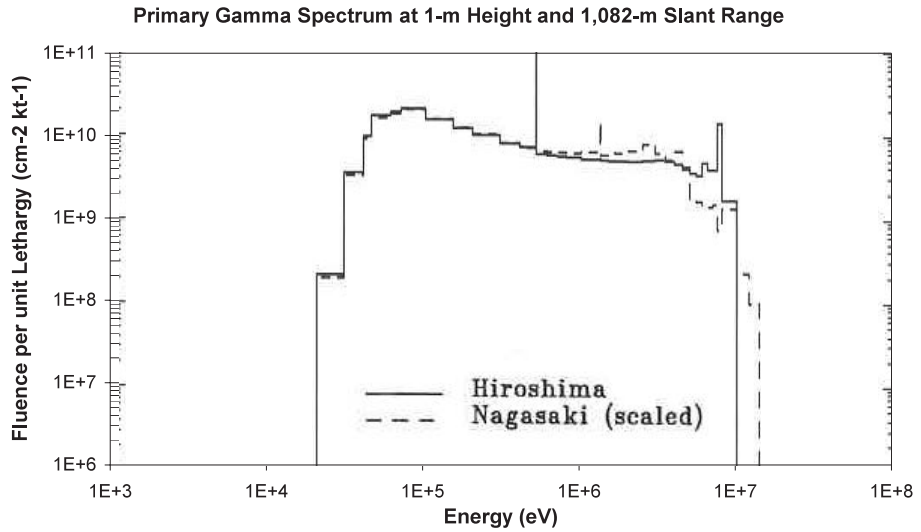

Figure 20. *Comparison of Hiroshima and Nagasaki prompt gamma-ray fluence per unit lethargy vs. neutron energy at a slant range of 1,082 m.*

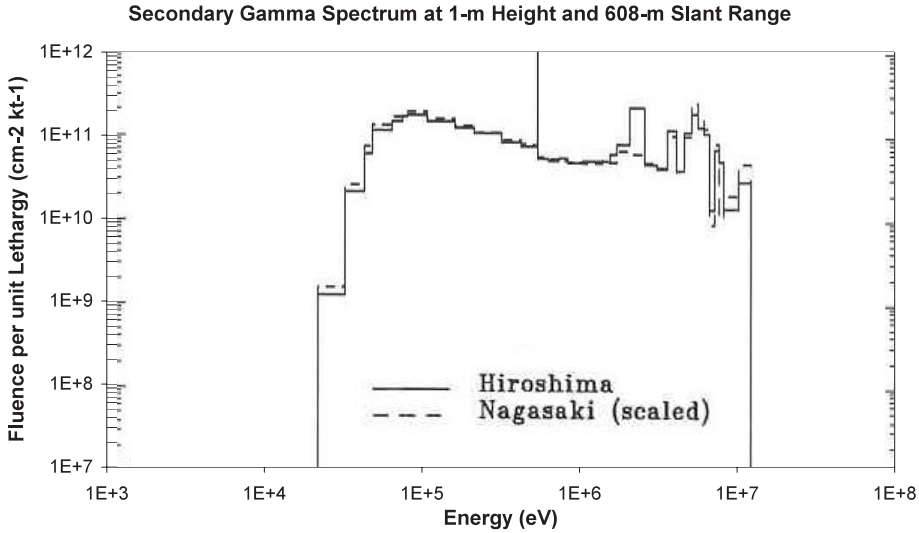

Figure 21. *Comparison of Hiroshima and Nagasaki secondary gamma-ray fluence per unit lethargy vs. neutron energy at a slant range of 608 m.*

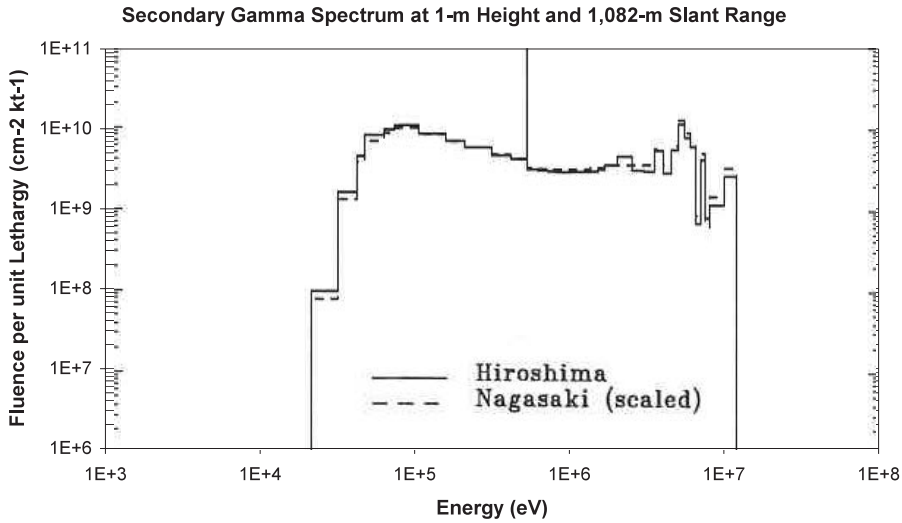

Figure 22. *Comparison of Hiroshima and Nagasaki secondary gamma-ray fluence per unit lethargy vs. neutron energy at a slant range of 1,082 m.*

The primary gamma-ray spectra shown in Figures 19 and 20 at 608- and 1,082-m slant ranges, respectively, have the same shapes at gamma-ray energies below about 5×10^6 eV. In the spectra at 608-m slant range, the Nagasaki spectrum shows more high-energy photons than Hiroshima, and the shapes of both spectra are similar to the weapon leakage spectra. At a slant range of 1,082 m, the spectra are basically the same for gamma-ray energies up to a few MeV. The Nagasaki weapon produces more higher-energy primary gamma-rays than the Hiroshima weapon.

The secondary gamma-ray fluence per unit lethargy for both weapons shown in Figures 21 and 22 are, for all practical purposes, the same at all slant ranges. These gamma rays are produced from capture reactions of low energy epithermal and thermal neutrons in the air and ground. The spectra for neutrons in these energy ranges have the same shape and scaled magnitude as shown in Figures 17 and 18.

Monte Carlo Prompt Radiation Calculations

Monte Carlo prompt radiation transport calculations were performed using the MCNP4C computer code (Briesmeister 2000). One of the reasons for repeating the analysis of the prompt radiation using Monte Carlo methods was to provide validation of the discrete ordinates fluence and activation calculations. MCNP is a general-purpose Monte Carlo code for neutron, gamma ray or electron transport in arbitrary three-dimensional configurations of materials bounded by first- and second-degree surfaces and fourth-degree elliptical tori. Briesmeister (2000) gives a complete description of the code and auxiliary routines and cross-section data used.

In the Monte Carlo method, simulating the random nature of particle interactions in a medium generates particle histories (tracks). The probability that a particle of a given energy is absorbed, scattered or reacts in a specified volume can be estimated by calculating the fraction of all particles with the specified energy that are so affected in the specified volume. Using a large number of histories that are random in nature to approximate some average particle behavior is the essential feature of the Monte Carlo method. In the calculational process, the track length of a particle between interactions, the interaction types, changes in particle energy and direction, production of secondary particles are monitored from the birth of the primary particle to the time it is absorbed or escapes from the problem geometry. Complete descriptions and discussion of the Monte Carlo method can be found in the publications of Kalos (1981), Spanier and Gelbard (1969), and Carter and Cashwell (1975).

Neutrons can be transported over energies from 10^{-11} to 20 MeV and gamma rays from 1 keV to 1,000 MeV. Continuous-energy, point-wise cross-section data based on ENDF/B-VI are used in the calculations. For neutrons, all reactions in a particular cross-section evaluation are taken into account. Thermal neutrons are described by free gas and S(α,β) models. For gamma rays, MCNP takes into account coherent and incoherent scattering, the possibility of fluorescent emission of annihilation radiation and bremsstrahlung.

Details of the Monte Carlo Calculations

The Monte Carlo calculations were performed with the same geometry configuration used in the discrete ordinates analysis and shown in Figure 3. Neutron and gamma-ray fluences were

estimated using cell fluence tallies at different distances from the epicenter. The transport was performed using ENDF/B-VI cross sections.

The weapon sources were located on the axis of symmetry above the ground plane at 600 m for the Hiroshima weapon and 503 m for the Nagasaki weapon. Neutrons and gamma rays emanating from the weapons were determined by sampling from the spectral and angular distribution data for the weapons. In the case of the Hiroshima weapon, the weapon tilt relative to the normal to the ground plane was accounted for to correctly describe the anisotropic distribution of the leakage radiation. In the case of the Nagasaki weapon, the neutron and gamma-ray leakage is isotropic, so it is not necessary to account for its tilt.

Fluences were calculated at 1 m above the ground and folded with kerma and activation response functions. Calculations were typically run for ten million source neutrons using a low energy neutron cut-off of 10^{-11} MeV to correspond with the lower energy bound of the multigroup cross sections used in the DORT calculations. Fractional standard deviations in the neutron fluences between 0 and approximately 700 m ground range were less than 1%. At greater distances, the uncertainties in the calculations increase to 5 to 15%. The statistical fluctuations in the data at ground ranges beyond approximately 700 m do not significantly impact trends in the neutron and gamma-ray dose and activation responses. If necessary, the statistics at long ranges can be improved by increasing the number of source particles (longer running times) or by incorporating variance reduction schemes such as particle splitting or additional source biasing.

Comparisons of Discrete Ordinates and Monte Carlo Calculations

The calculated Hiroshima ^{60}Co and ^{152}Eu and Nagasaki ^{60}Co and ^{32}P activation obtained using Monte Carlo and discrete ordinates methods are compared as a function of slant range in Figures 23 and 24, respectively. The results of the Hiroshima discrete ordinates calculations are compared with two different Monte Carlo calculations. One was performed at ORNL using the model and scoring procedure described above and a second was performed at LANL using a different model and scoring scheme. The Nagasaki discrete ordinates calculations are compared with Monte Carlo calculations performed at ORNL.

The LANL MCNP calculation of the Hiroshima radiation environment was performed using an XYZ geometry designed to emphasize the activation responses about the hypocenter and to analyze the anisotropic activation on the ground when the Hiroshima weapon was tilted. In the geometry, 40 m $\times$ 40 m $\times$ 2 m cells were constructed above a 50-cm-thick ground layer. The air and ground regions extended $\pm$535 m in the X and Y directions. The air extended to an altitude of 1,500 m in the Z direction.

The air and ground compositions used were the same as those in the DORT calculation with the air also modeled in seven altitude dependent layers having compositions corresponding to those in Table 3. The transport and activation cross sections were taken from the ENDF/B-VI (Ver. 2).

The Hiroshima neutron source was represented using detailed angle and energy resolved spectra that were binned into the same angle and energy structure used in the DORT calculations. The weapon was not tilted for these MCNP or DORT calculations. The neutron fluence was estimated in the geometry using cell fluence tallies and folded with the activation cross sections to assess the ^{60}Co and ^{152}Eu production. Calculations were performed for more than 30 million

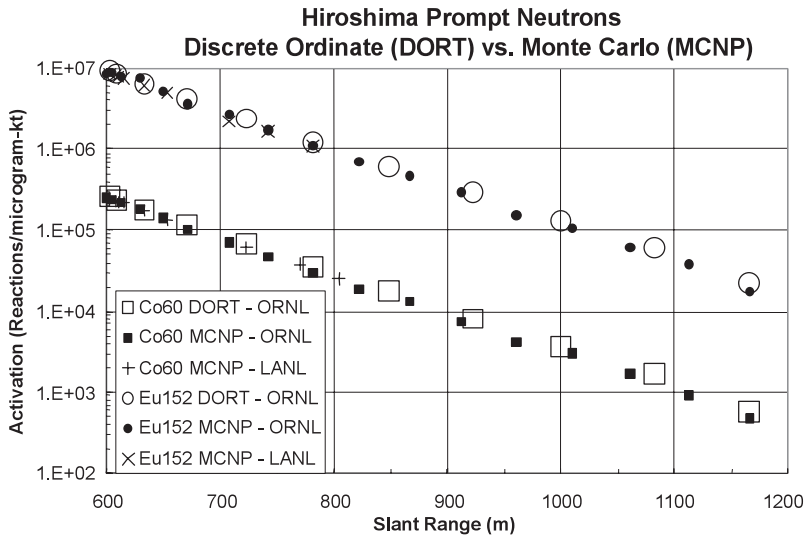

Figure 23. *Comparison of DORT and MCNP calculations of Co and Eu reaction rates (Hiroshima weapon).*

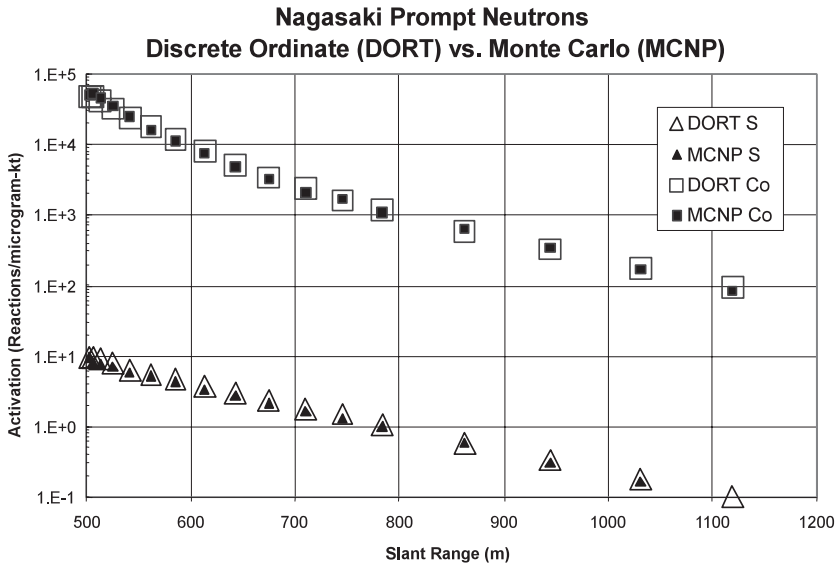

Figure 24. *Comparison of DORT and MCNP calculations of Co and S reaction rates (Nagasaki weapon).*

source neutrons resulting in less than 2% fractional standard deviations in the calculated ^{60}Co and ^{152}Eu activation for slant ranges between 600 and approximately 800 m. The large source sampling by LANL was made to accurately calculate the ^{32}S fast neutron responses about the hypocenter. The thermal neutron activation was calculated simultaneously using a neutron energy cutoff of 10^{-11} eV.

The Monte Carlo and discrete ordinates estimates of the Hiroshima ^{60}Co and ^{152}Eu and Nagasaki ^{60}Co and ^{32}P activation are in excellent (<10%) agreement. The comparison of ^{32}P activation for Nagasaki shown in Figure 24 was included to compare the calculation of fast neutron transport at Nagasaki. There were no fast neutron activation measurements made at this city, so the only validation of the discrete ordinates transport of energetic neutrons is through this comparison.

The reproduction of the range dependent activation by the Monte Carlo calculations lends considerable credibility to the discrete ordinates calculations of the activation responses. These data corroborate the validity of the multigroup transport cross sections used in the discrete ordinates calculations. The MCNP code uses continuous cross section data that more accurately treat resonances. The multigroup energy bins often result in an approximate treatment of the resonance when the cross sections are averaged over the group width. The angular dependence of the leakage radiation from the weapons in the discrete ordinates is approximated through the choice of the Legendre expansion of the cross-section data and in the choice of angular quadrature. The MCNP code uses a much finer approximation for angular scattering. The P_3 Legendre expansion used in the DOORS code system to account for scattering and the choice of the 240-angle quadrature provides suitable results for the neutron and gamma-ray transport at both cities.

Further details of the DORT and MCNP comparisons can be found in Santoro et. al. (2001).

Discussion of Results

Many of the concerns expressed over the validity of the calculations carried out in support of the DS86 study are now resolved. The Hiroshima and Nagasaki prompt radiation in the air-over-ground geometry are well described by the discrete ordinates transport calculation sequence. The agreement between the discrete ordinates and Monte Carlo transport calculations provide a consistent description of the neutron environment at 1 m above the ground, where measured and calculated activation and inferred dose data are compared. ENDF/B-VI fine group cross-section data, in combination with a high order quadrature, provide an excellent characterization of the neutron and gamma-ray fluence distributions in the air-over-ground geometry.

Part B. Delayed Radiation

The delayed radiation from the Hiroshima and Nagasaki bombs contribute to the neutron and gamma-ray doses and activation at all distances. Delayed radiation is generated by the emission of neutrons and gamma rays from fission products in the fireball. The low air density in the fireball enhances the transport of these particles and results in their becoming a large contribution to the radiation fluences. For example, delayed radiation contributes more than one-half of the gamma-ray dose out to 1,500 m slant distance at both cities. At Hiroshima, the delayed neutrons add less than 10% to the dose and thermal activation and less than 5% to fast neutron activation at all ranges. However at Nagasaki, the delayed neutrons are significant, having their maximum contribution to thermal neutron activation (approximately 60%) at about 700 m slant range and to the neutron dose (approximately 40%) at the hypocenter. The delayed neutron contribution drops rapidly at distance, and at 2,500 m, it contributes less than 5% to either neutron dose or thermal neutron activation. Delayed neutrons contribute less than 10% to the Nagasaki fast neutron activation at all ranges.

The delayed radiation reported in DS86 was recalculated in 1993 (Kaul et al. 1994) and again in 2002 for this study using transport codes and methods similar to those used in the prompt radiation transport calculations described in this chapter. The results of the 1993 delayed neutron calculations and the results of the delayed gamma calculations carried out in 2002 are used for the delayed radiation fluences given in this chapter. The major differences between the DS02 and the DS86 delayed radiation calculations are summarized in Table 7.

The improved methods used to calculate the delayed radiation for this work were also used to improve the analysis of several Nevada and Pacific test shots. For those test shots, calculated activation results were compared with measurements of time-dependent and time-integrated neutron and gamma measurements. For example, calculations of time-dependent delayed gamma radiation of the Pacific test shot King (Kaul and Egbert 1991) showed good agreement with measurements. It was demonstrated that by using 2-D source hydrodynamic models, perturbations from the passing air shock, the formation of the triple point, and the dispersion of

Table 7. Differences between DS86 and DS02 delayed radiation calculations

DS86	DS02
Time Dependent Source	
Neutrons: Augmented Maxwellian Spectra to 2.5 MeV Gamma Rays: Empirical Spectra	Neutrons: ENDF/B-VI Spectra to 8 MeV Gamma Rays: ENDF/B-VI Spectra
Time Dependent Geometry	
Line-of-Sight Optical Depths (g cm^{-2}) from 2-D Air Density Contours Contours from STLAMB Hydrodynamic Code	2-D Air Density Contours Contours from STLAMB Hydrodynamic Code
Transport Codes	
ANISN Transport in Air 300 Time Steps ANISN Transport in Hydrodynamically Perturbed Air MORSE Fluence Perturbation due to Air-Ground Interface DLC-130 (DABL) ENDF/B-V cross sections	DORT Transport in Air-over-Ground Delayed Neutrons use 12 Time Steps with Vitamin E ENDF/B-VI cross sections Delayed Gamma Rays use 18 Time Steps with DABL-69 ENDF/B-VI cross sections

source at late times the delayed radiation can be adequately modeled. Another study (Egbert 1995) of the Nagasaki-like Nevada test shots Ranger Fox, Buster-Jangle Charlie and Buster-Jangle Dog showed good agreement for total fast (^{32}S) and thermal (^{197}Au) neutron activations. A comparison showed that over all ranges the total prompt and delayed neutron calculations were consistent with measurements. The measurement to calculation ratio for ^{197}Au was a nearly constant ratio of 1.2 for all shots over ranges 0 to 2,000 m. The measurement to calculations ratio for ^{32}S was a nearly constant ratio of 1.25 over ranges 0 to 1,500 m for Charlie and Dog. There were no ^{32}S measurements for Ranger Fox. Figures 25, 26, and 27 show the measurements compared to calculations for these three test shots. This study did not reach a conclusion as to why there was a 20% under prediction of the activation. However, it is a fact that the calculated fast neutron activation and the sum of the calculated prompt and delayed thermal neutron activation, each with very different relaxation lengths, is nearly proportional to their measurements at all ranges. This suggests that the problem is likely due either to measurement normalization, possibly involving the cross section used for sulfur activation in these early weapon tests, or to the neutron source normalizations.

The gamma-ray doses for two Nevada Test shots, Ranger Fox and Buster Jangle Dog, have also been recalculated using the DS02 delayed methodology. They had first been calculated using the DS86 methodology for the DS86 Final Report (Roesch 1987), and those results are shown on pages 128 to 130 in that report. The current delayed calculation results are combined with a recent LANL Monte Carlo calculation of the prompt gamma-ray doses and compared with the measurements. This is shown on Figures 28 and 29 for Fox and Dog respectively. The results show acceptable agreement with Fox for both the magnitude and the rate of falloff with distance. For Shot Dog, the measured and calculated doses also fall off at about the same rate with distance, but the measurements are consistently 50% larger than the calculations, while at Fox

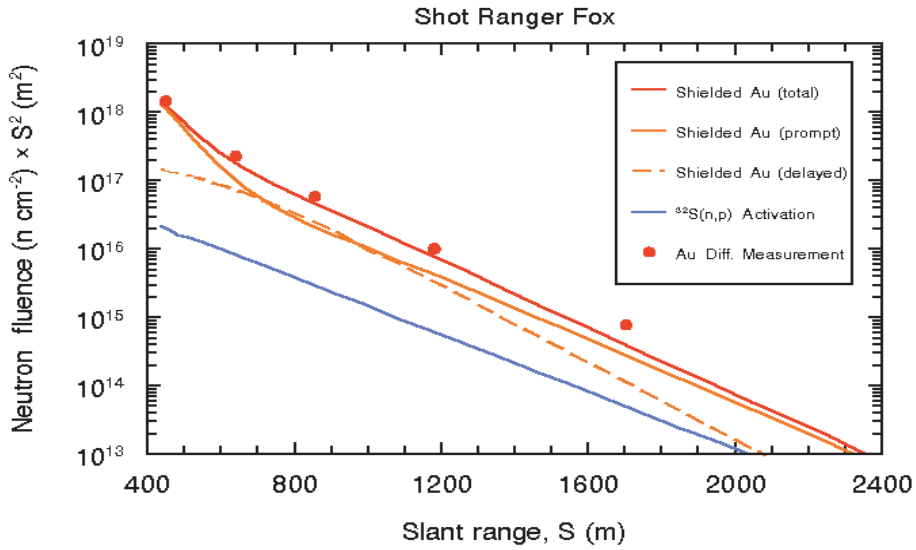

Figure 25. *Comparison of neutron measurements and calculations at Ranger Fox.*

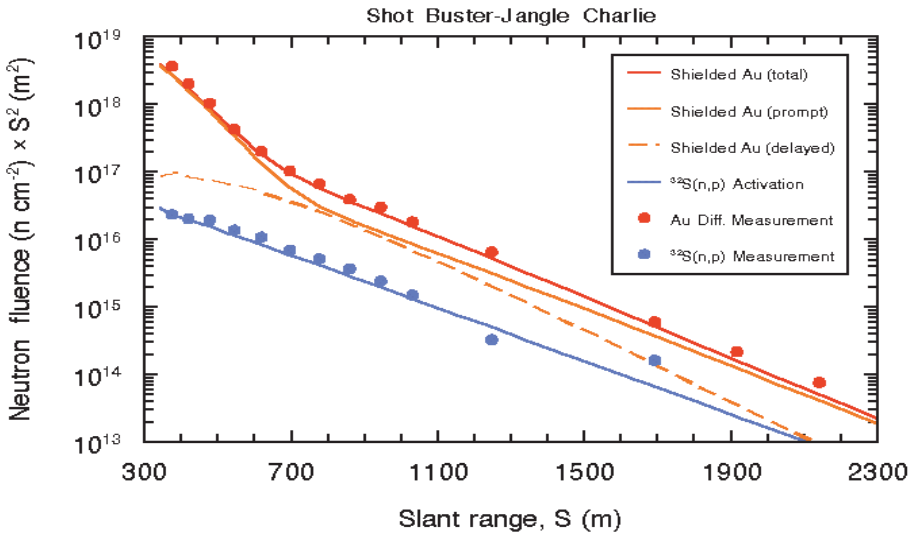

Figure 26. *Comparison of neutron measurements and calculations at Buster-Jangle Charlie.*

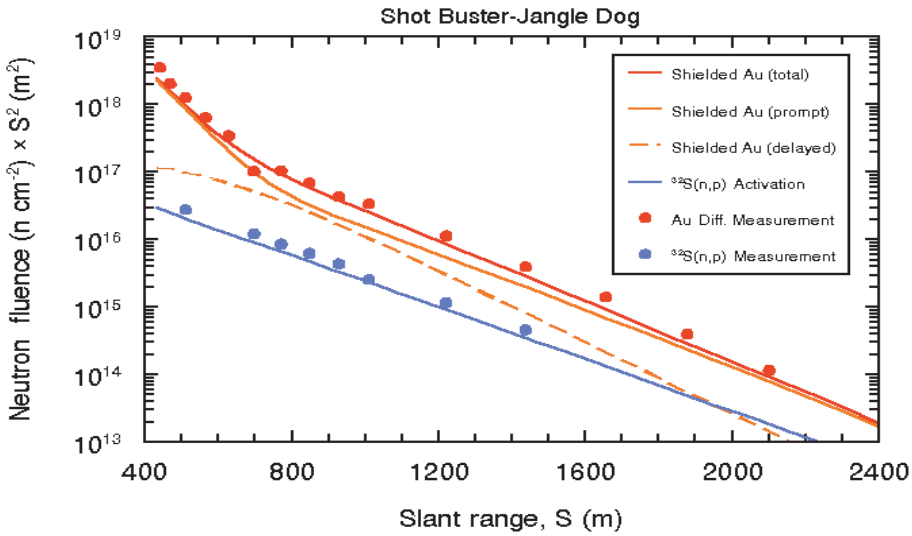

Figure 27. *Comparison of neutron measurements and calculations at Buster-Jangle Dog.*

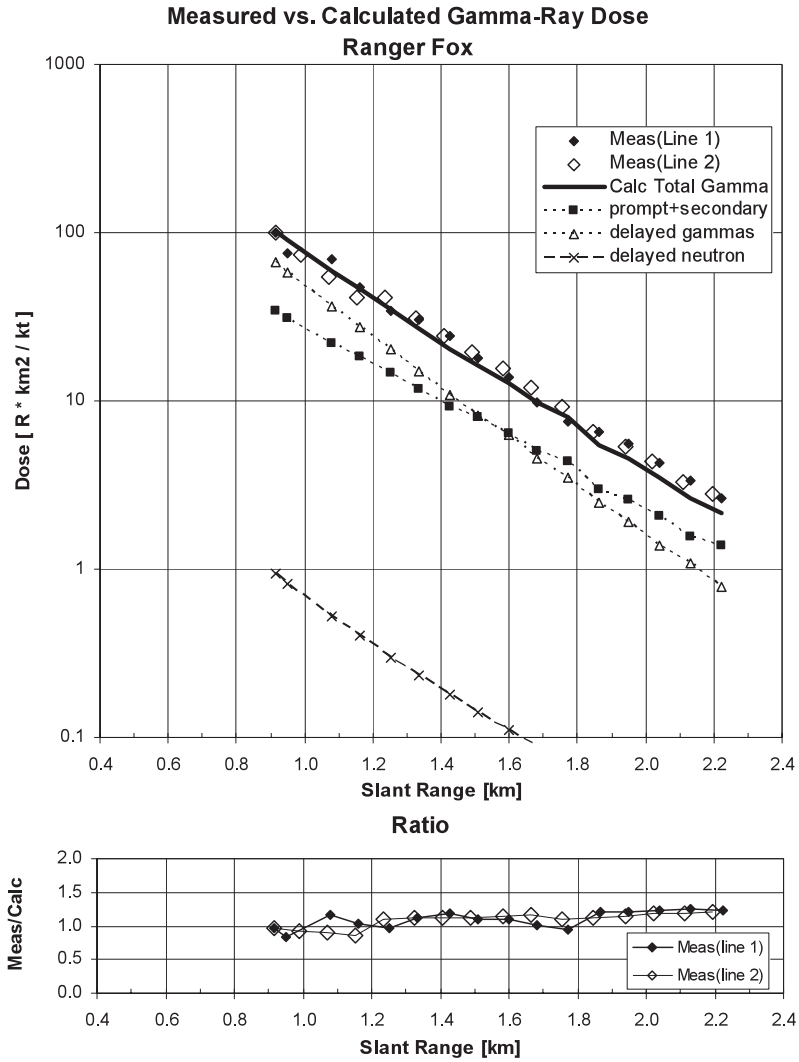

Figure 28. *Comparison of gamma-ray measurements and calculations at Ranger Fox.*

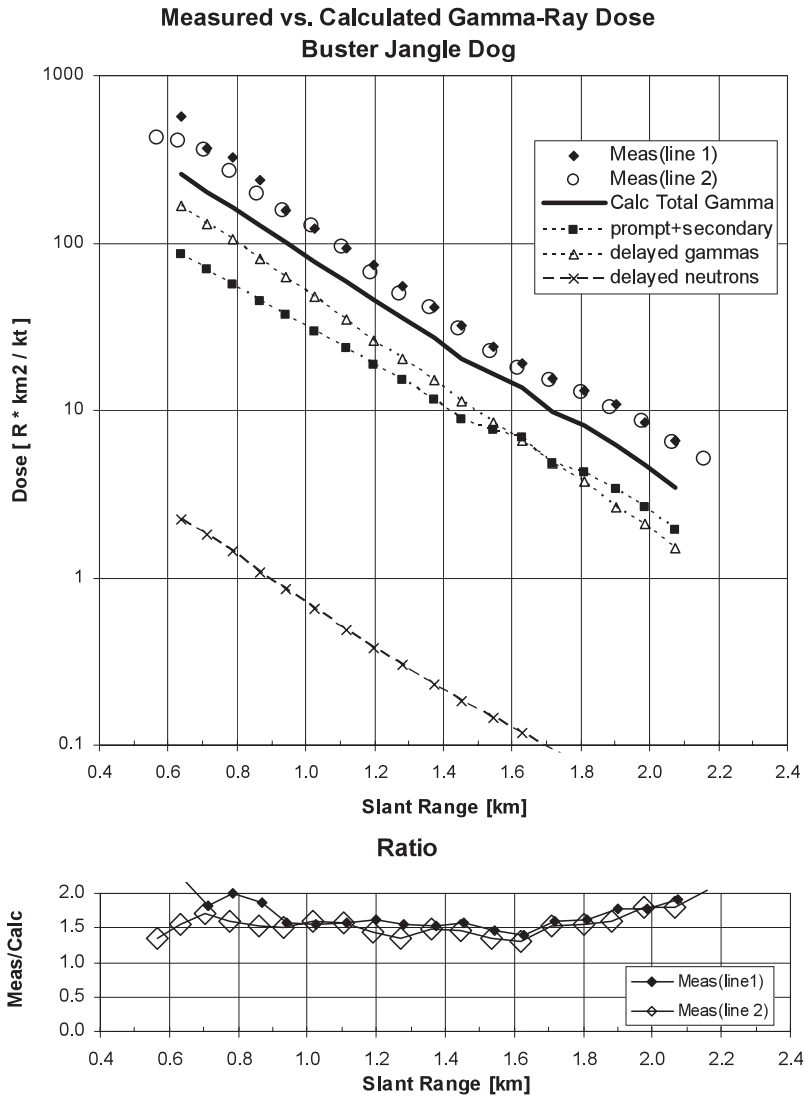

Figure 29. *Comparison of gamma-ray measurements and calculations at Buster-Jangle Dog.*

they are about 15% larger. The calculated prompt and delayed gamma-ray doses each have significantly different relaxation lengths, yet the sums are proportional to their measurements. A definitive explanation for the Dog discrepancy has not been found. However, it has been suggested that either downward corrections should be made in the measured values based on possible calibration problems in these measurements (Storm 1981), or that the source normalizations may be slightly low.

Source Location and Air Density Perturbations due to the Fireball

The delayed radiation calculations were carried out using R-Z cylindrical densities of the air at a series of times after the burst. In DS86, the air density for the delayed radiation was calculated out to 3,000 m ground range and 2,000 m above the ground using the code STLAMB (Dean 1982). STLAMB is a variant of the LAMB code developed by Needham and Wittwer (1975). STLAMB was used in DS86 to calculate the mass thickness of air along a line from a point 1 m above the ground back to the source at the center of the fireball. A homogenous air transport calculation generated fluences as a function of this distance and mass thickness. A correction factor was applied to account for the non-homogeneous distribution of reduced air density in the fireball. An energy-angle correction factor was used to account for radiation scattering from the ground. The DS86 delayed fluences were generated at 1-m height for ground ranges between 100 to 2,500 m in 25 m steps.

By 1993, new methods for calculating delayed radiation became available due to increased computational capability of computers that markedly decreased the execution time of radiation transport codes. The expanding fireball and rising source following the weapon detonation was modeled in a series of snapshots for use in multiple DORT calculations. At each time step, the code STLAMB was used to calculate the two-dimensional air density at the mesh points used in the delayed radiation DORT calculations. The ATR code (Kaul et al. 1992), which models air hydrodynamics, source rise, delayed source spectra, one-dimensional radiation transport, and two-dimensional ground correction factors, was used to estimate the dose in fine time steps at typical survivor distances. From these results, eighteen geometrically increasing time steps were chosen as snapshot candidates. The time steps included a 1.00 second snapshot and the remaining times of subsequent snapshots differed by $2^{1/2}$. Twelve time snapshots were chosen for the DORT calculations so that no more than 10% of the dose would arise from any single time step. Table 8 shows time steps and time boundaries used in the calculations for delayed neutrons and delayed gammas.

Table 8 also shows the proportion of dose that was received in each time interval according to the ATR code. Note that the delayed neutron dose arrives earlier than the delayed gamma dose. For delayed neutrons, several intervals were combined to achieve an equal distribution of dose within each time interval. By 2002, increased computational power permitted all time steps to be utilized for the delayed gamma-ray calculations. An illustration of the current Hiroshima and Nagasaki profiles, at 2 seconds, are shown in Figures 30 and 31, respectively. Many other examples of the Hiroshima and Nagasaki air density profiles, calculated with STLAMB, are given in the DS86 Final Report, Volume 2, Figures 41 to 52, pages 81 to 86 (Roesch 1987).

The fission product source was placed at the location of the highest temperature of the fireball. When this location was along the centerline of the fireball, the source was represented as a point, and the GRTUNCL code was used to calculate an uncollided fluence-first collision

Table 8. Time steps, prorated dose estimates, height of source for delayed radiation calculation

Time steps	Start (sec)	End (sec)	Mid (sec)	ATR % DN	Selected DN	ATR % DG	Selected DG	Hiroshima Height'86 Height'93	Nagasaki Height'86 Height'93	Hiroshima Height'02	Nagasaki Height'02	Source shape
1	0	.0743	.0625	7%	X	3%	X	580	503	600	503	Point
2	.0743	.1051	.0884	3%		1%	X	580	503	600	503	Point
3	.1051	.1487	.125	4%	X	2%	X	580	503	600	503	Point
4	.1487	.2102	.1768	6%		2%	X	580	503	600	503	Point
5	.2102	.2973	.2500	6%		3%	X	580	503	600	503	Point
6	.2973	.4204	.3536	9%	X	5%	X	580	503	600	503	Point
7	.4204	.5946	.5000	10%	X	5%	X	580	503	600	503	Point
8	.5946	.8409	.7071	11%	X	8%	X	580	503	602	504	Point
9	.8409	1.189	1.000	10%	X	8%	X	590	503	607	508	Point
10	1.189	1.682	1.414	10%	X	12%	X	600	512	620	519	Point
11	1.682	2.378	2.000	8%	X	11%	X	670	640	644	542	Point
12	2.378	3.364	2.828	9%	X	10%	X	725	712	688	586	Point
13	3.364	4.757	4.000	3%	X	8%	X	812	812	760	660	Point
14	4.757	6.727	5.657	2%		8%	X	937	~937	868	772	Torus
15	6.727	9.513	8.000	1%	X	6%	X	988	~988	1025	936	Torus
16	9.513	13.45	11.314	1%		3%	X	~1170	~1170	1249	1169	Torus
17	13.45	19.03	16.000	<1%		3%	X	1500	~1500	1551	1486	Torus
18	19.03	30.00	22.624	~0%		2%	X	~1700	~1730	1947	1904	Torus

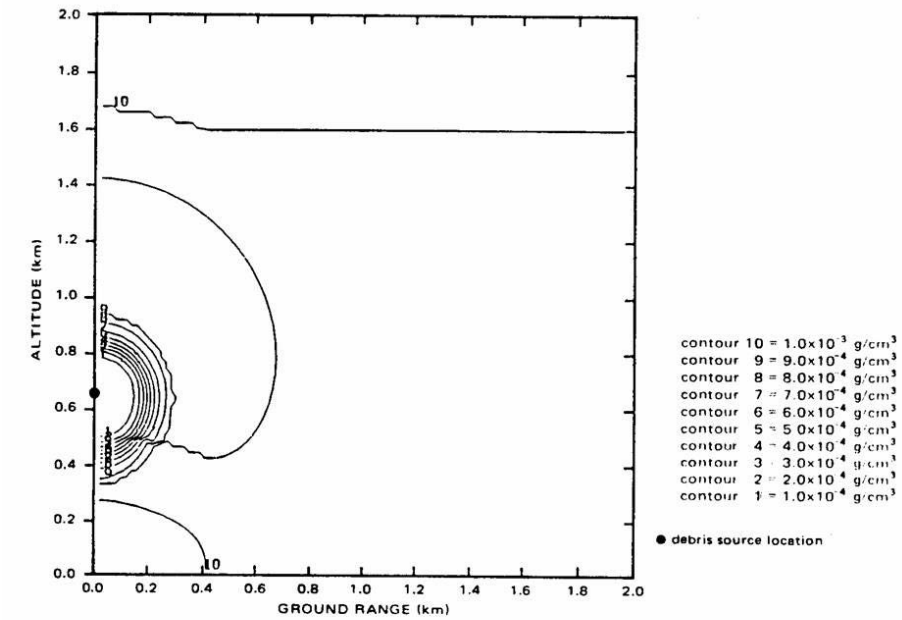

Figure 30. *Iso-contours of air density at Hiroshima 2.028 seconds after the explosion.*

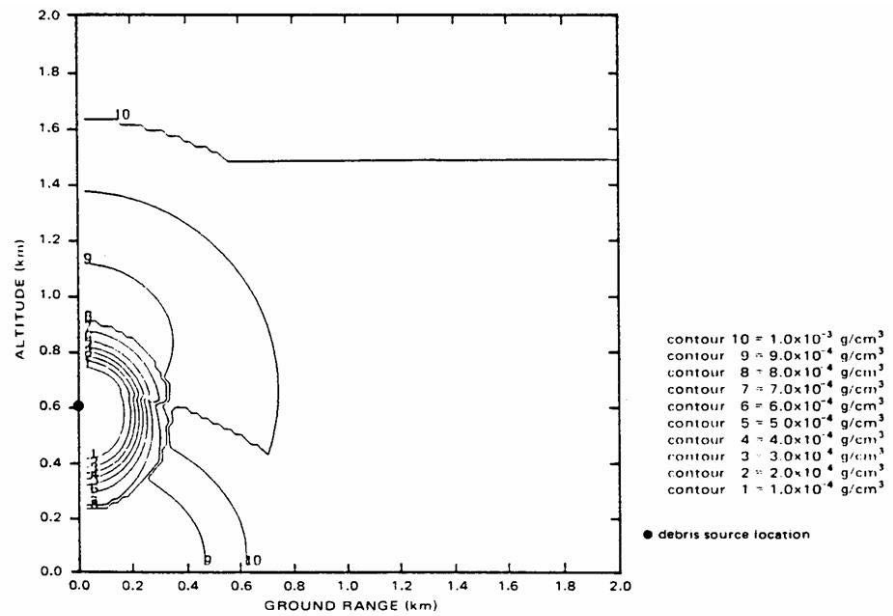

Figure 31. *Iso-contours of air density at Nagasaki 2.028 seconds after the explosion.*

source for DORT (DOORS3.2 1998). As explained above, the first collision source reduces the ray effects that occur in discrete ordinate air-over-ground calculations. At times greater than 5 seconds, the highest temperature location moves off the centerline and forms a torus. This toroidal source was distributed proportional to the temperature distribution of the fireball and input directly into the DORT code. The GRTUNCL code is not able to calculate the first collision source and uncollided fluence for a distributed source, thus there are more ray effects observed with the toroidal source. At 8 seconds after the Hiroshima explosion, the toroidal source extended throughout many radial mesh intervals. The hot locations were in a ring of 250 m radius and 1,025 m height. Most of the locations were within ±50 m of this ring.

Delayed Neutron Source

The DS02 delayed neutron source was obtained from the ENDF/B-VI fission product library of neutron and gamma emission spectra from a Los Alamos National Laboratory report (England et al. 1988). This report contains:

- Delayed neutron yield rates for ^{235}U, ^{238}U, and ^{239}Pu fast fission
- Total delayed neutron rate vs. cooling time for ^{235}U, ^{238}U, and ^{239}Pu fast fission at 39 time steps (0, 0.1, 0.2, 0.3, 0.4, 0.5, 1.0, 1.5, ... 5, 6, ... 10, 15... 60, 70... 120, 180, 240, 300 seconds)
- Fraction of delayed neutrons with energies above E for ^{235}U, ^{238}U, and ^{239}Pu fast fission in 0.5-MeV increments up to 10 MeV at 8 times steps (0, 1, 2.5, 10, 15, 20, 30 and 60 seconds)

Figure 32, reproduced from the LANL report, shows the total neutron emissions per second for eight different fissile isotopes, and Figure 33 shows the cumulative spectra for ^{235}U. The neutron source spectra given in the LANL report were converted into the Vitamin-E energy group structure at each snapshot time. The energy resolution of the data given in the LANL report is much coarser than the fine group Vitamin-E.

The DS86 delayed neutron source was based on the standard six delayed neutron groups, each with a half-life, total number of neutrons and a Maxwellian temperature to form a time-dependent energy spectrum. This was based on data from LANL. In 1986, as DS86 was about to be installed at RERF, the preliminary LANL report showed a larger neutron source above 1 MeV. Based on this information, an energy-dependent correction was applied in DS86 to match the preliminary LANL delayed neutron source up to 2.5 MeV. This formed the DS86 delayed neutron source. The DS86 source did not extend above about 2.5 MeV.

Delayed Gamma Source

The delayed gamma source used in DS02 was initially used in a 1993 calculation. The delayed gamma source was generated from initial fission product yields made available by LANL (Katakura and England 1991). The gamma emission spectra used an improved version of ORIGEN2 developed by Roberts (1996) that generated gamma spectra at the required times. The spectra were regrouped into Vitamin-E format. Figure 34 shows a comparison between the Akiyama and An (1982) ^{235}U fast fission products measurements and the ENDF/B-VI spectra used in DS02. The Akiyama and An measurements formed a basis for the DS86 Hiroshima delayed gamma source. However, as seen in the figure, these measurements start at about 20 seconds, which is after the important delayed gamma rays are emitted.

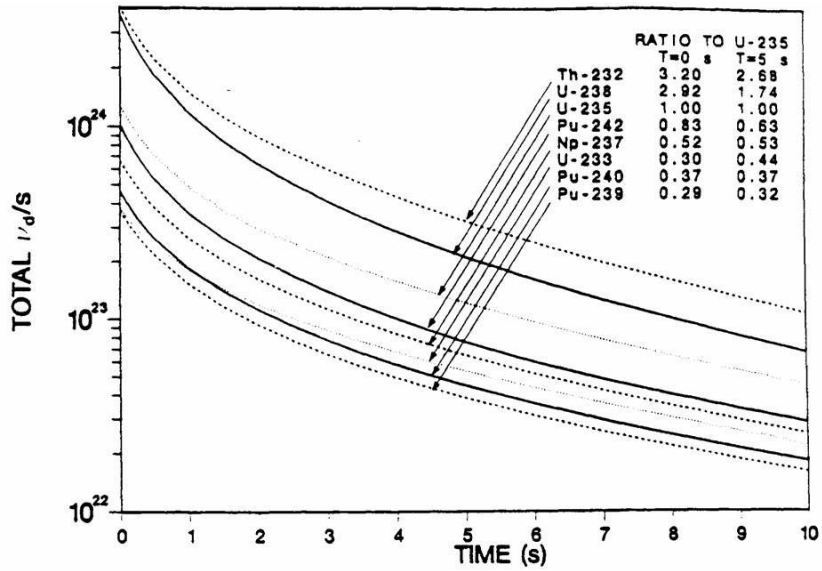

Figure 32. *Total ν_d/s for eight fuels vs. time (s) for fission pulse of 1.3 × 10^{26} fission over 10^{-4} seconds (England et al. 1988).*

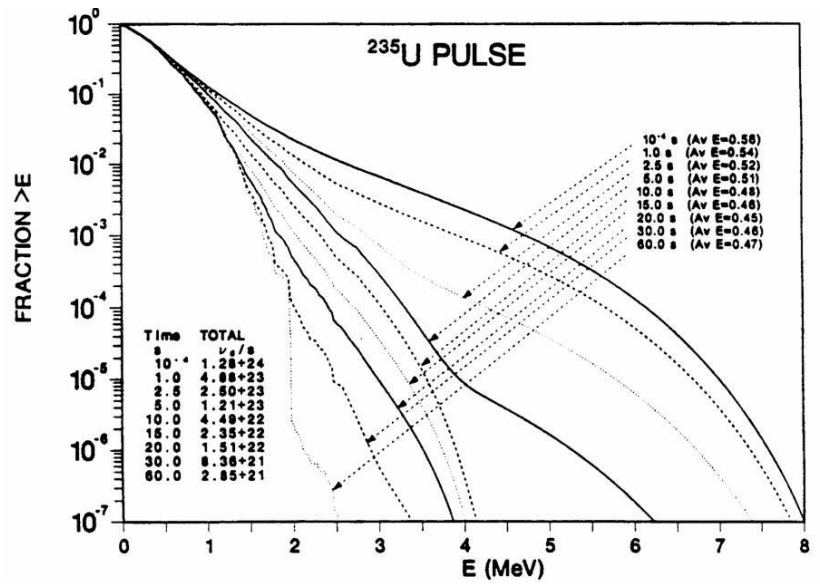

Figure 33. *^{235}U fraction of total delayed neutrons >E (England et al. 1988).*

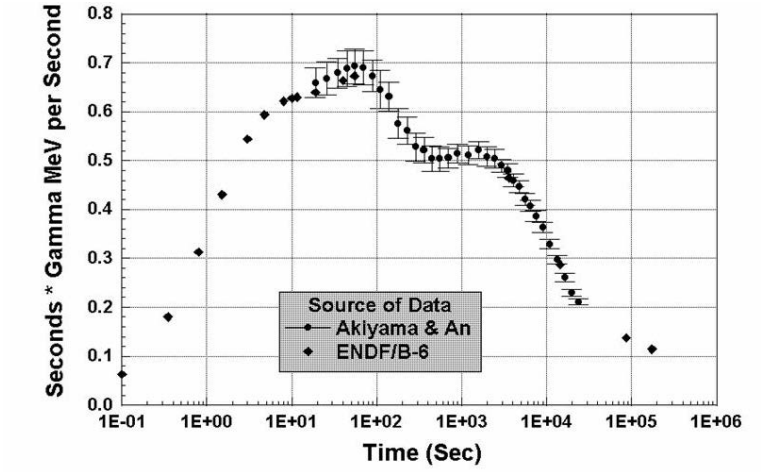

Figure 34. *^{235}U fast fission product gamma ray emission rate.*

The Hiroshima ^{235}U delayed gamma fission source was first used in 1993 to calculate fluences. The results were similar to the DS86 delayed gamma results. Because of this preliminary agreement and constraints of time and budget, the Nagasaki ^{238}U and ^{239}Pu (20% and 80%) delayed gamma fluences were not recalculated in 1993. It was expected that there would be little change. In 2002, the delayed gamma rays were recalculated for both Hiroshima and Nagasaki using the same methods used in 1993. However, a different version of STLAMB was used in these calculations, because the version of the code used in 1993 could not be reconstructed. The version of STLAMB used for the DS02 delayed gamma rays had a slightly smaller fireball rise after the reflected shock passes through the fireball than did the 1993 version. Table 8 shows the different fireball heights. At times between 2 and 4 seconds there is a 50-150 m difference in heights between the codes. This difference in fireball heights results in an uncertainty in the delayed gamma-ray dose, which is largest near the hypocenter. Also, the location of the source within the fireball is uncertain. Issues concerning the debris source such as the length of time the debris source remains near the center of the fireball, whether or not the source fills the fireball, and whether the debris source rises to the top of the fireball more rapidly have all been debated by Working Group members. However, about half of the delayed gamma-ray dose arrives before the fireball moves from its initial height. Furthermore, survivors are at distances from the bomb where the fireball rise is less important to dose uncertainty. In the extensive discussion about delayed gamma rays in Chapter 3, Appendix 4 of the DS86 Final Report, Volume 2 (Roesch 1987), it was pointed out that in Hiroshima and Nagasaki the initial scaled height of the debris source was higher than that of the nuclear tests used to evaluate the delayed radiation calculations, reducing the uncertainties in Hiroshima and Nagasaki compared to the nuclear tests. Given that the delayed gamma rays contribute approximately half the total dose to survivors in Hiroshima and Nagasaki, and the delayed radiation is the largest remaining uncertainty in the free-field calculations, in the future it may be desirable to perform modern fireball calculations. This could be accomplished by placing the debris source in a range of locations within the fireball by coupling the 2-D LANL bomb hydrodynamic results with a modern 2-D fireball hydrodynamics code.